EasyChair Preprint

№ 15400

Development of an Optical Communication System for Underwater Robots

Gabriel Lopes, Humberto Silva, Aléxis K. Uenojo, Ettore De Barros and Eduardo Lorenzetti Pellini

EasyChair preprints are intended for rapid dissemination of research results and are integrated with the rest of EasyChair.

November 8, 2024

Development of an Optical Communication System for Underwater Robots

Gabriel S. V. Lopes [*] **Humberto T. Silva** [**] **Aléxis K. Uenojo** [***]
Ettore A. Barros [****] **Eduardo L. Pellini** [†]

[*] *Programa de Pós Graduação de Engenharia Elétrica, Escola Politécnica da Universidade de São Paulo, SP (e-mail: gabriel.souza.lopes@alumni.usp.br).*
[**] *Laboratório de Veículos Não Tripulados, Departamento de Engenharia Mecatrônica, Escola Politécnica da Universidade de São Paulo, SP (e-mail: htrindade.silva@gmail.com).*
[***] *Programa de Pós Graduação de Engenharia Mecatrônica, Escola Politécnica da Universidade de São Paulo, SP (e-mail: alexis.uenojo@usp.br).*
[****] *Departamento de Engenharia Mecatrônica, Escola Politécnica da Universidade de São Paulo, SP (e-mail: eabarros@usp.br)*
[†] *Departamento de Energia e Automação, Escola Politécnica da Universidade de São Paulo, SP (e-mail: elpellini@usp.br)*

Abstract: Underwater robots are widely employed in exploration and intervention missions in oceans, seas, rivers and lakes. Wireless data transmission in underwater environments is one of the biggest challenges presented in the development of robotic systems, since the use of Radio Frequency (RF) is practically unfeasible due to the high attenuation imposed by the environment. Underwater optical modems are great alternatives for solving this issue, as they allow for the establishment of communication links with MHz frequency band at distances of up to a hundred meters. The development of unidirectional devices is discussed and the system general functioning is evaluated, in a hyperbaric chamber, through the transmission of a data stream, with emphasis on the maximum band reached and the Bit Error Rate (BER) measured.

Keywords: Underwater optical modem; SiPM; Underwater communication; Underwater robots.

1. INTRODUCTION

The oceans cover about two-thirds of the Earth's surface and directly impact human existence. However, due to their extremely complex nature, they have been sparsely explored (Yuh et al., 2011). Currently, these environments are being studied through the use of robots and sensors, allowing for reduced operational costs and decreased risks to human lives. Additionally, robotics enables an expansion of mission coverage area, as the depth limits and submersion times of equipment surpass those of divers (Lehman, 2018).

Marine robotics poses several challenges not present in terrestrial and aerial robotics fields, often hindering the transfer of solutions between areas (Zhang et al., 2015). One of the major challenges lies in wireless data transfer, which can be achieved through Radio Frequency (RF), acoustic or optical waves.

Given the attenuation suffered by radio frequency waves in the underwater environment, mainly due to the high conductivity of the medium, and the bandwidth limitation related to data transmission via acoustic waves, the use of optical communication in specific applications becomes attractive where the exchange of larger data quantities at short to medium distances, around tens of meters, is required (Gussen et al., 2016).

Equipments with cameras and sensors fixed to underwater structures often remain for extended periods, storing vast amounts of data. The use of such equipments allows for the environment oceanographic study, which is often mandatory, such as in the case of a concession for the construction of an oil exploration platform (Mariano and La Rovere, 2007).

Autonomous Underwater Vehicles (AUVs) and Remotely Operated Vehicles (ROVs), used in subsea inspection, monitoring, and intervention activities, can also be an important resource to collect this stored data without the need to retrieve a device from the ocean.

For this purpose, both anchored equipments and vehicles must have underwater devices capable of transferring significant amounts of information. To accomplish this task, the use of optical modems becomes suitable, as they enable a faster data capture.

Due to the high cost of these types of commercial products (introduced to the market just over six years ago) and the challenging acquisition of these devices due to possible embargoes by countries holding such technologies (List, 2017) (Union, 2016), it becomes interesting to research and develop national solutions for specific scenarios.

Section 2 discusses the optical communication channel in the underwater environment, while Section 3 presents the state of the art regarding optical modems. Section 4 outlines the development stages, and Section 5 discusses the experimental tests conducted. Finally, conclusions and future works are presented in Section 6.

2. OPTICAL COMMUNICATION CHANNEL IN UNDERWATER ENVIRONMENTS

Currently, optical fibers are widely used in telecommunications as a mean of propagation, enabling the establishment of high-speed connections in the Gbps range. Simpler devices, such as remote controls, use infrared Light Emitting Diodes (LEDs) and phototransistors to transfer commands and telemetry. An underwater optical modem shares similar characteristics with the mentioned systems. Among these, bandwidth stands out, which can exceed several MHz using suitable phototransmitter and photoreceiver components.

The attenuation coefficient of an electromagnetic wave in a given medium is defined in Equation (1) as the sum of the absorption coefficient α and the scattering coefficient β as a function of the wave angular frequency ω (Schirripa Spagnolo et al., 2020).

$$c(\omega) = \alpha(\omega) + \beta(\omega) \tag{1}$$

The absorption coefficient of an electromagnetic wave can be defined in Equation (2) (Balanis, 2012).

$$\alpha(\omega) = \omega\sqrt{\mu\epsilon}\left(\frac{1}{2}\left(\sqrt{1+\left(\frac{\sigma}{\omega\epsilon}\right)^2}-1\right)\right)^{0.5} \tag{2}$$

Where μ is the magnetic permeability, ϵ is the electric permittivity, and σ is the conductivity, all of which depend on the considered channel.

In air, one considers $\epsilon_{\text{air}} \approx 8.85 \times 10^{-12}$ F/m, $\mu_{\text{air}} \approx 4\pi \times 10^{-7}$ H/m, and $\sigma_{\text{air}} \approx 1 \times 10^{-12}$ S/m. Meanwhile, in underwater environments, for frequencies up to 1 GHz and under constant temperature and salinity conditions, one can consider $\mu_{\text{water}} \approx 4\pi \times 10^{-7}$ H/m, $\epsilon_{\text{water}} \approx 7.16 \times 10^{-10}$ F/m, $\sigma_{\text{water}} \approx 0.001$ S/m, and $\sigma_{\text{saltwater}} \approx 4$ S/m (Somaraju and Trumpf, 2006) (Schirripa Spagnolo et al., 2020).

Figure 1 illustrates the disparity between the absorption coefficients of electromagnetic waves across a broad spectrum of frequencies, propagated in air, freshwater and saltwater. Therefore, the unfeasibility of using RF in applications requiring high transfer rates in underwater environments, especially saline, is evident.

However, as frequencies approach those of visible light, in the order of hundreds of THz, the attenuation suffered by electromagnetic waves is drastically reduced, allowing for the propagation of visible light spectrum for tens or hundreds of meters in ideal situations (Tyler et al., 1998). This effect occurs mainly due to the conductivity and electric permittivity values of water, which can vary with the propagated wave frequency. In a simplistic manner, it

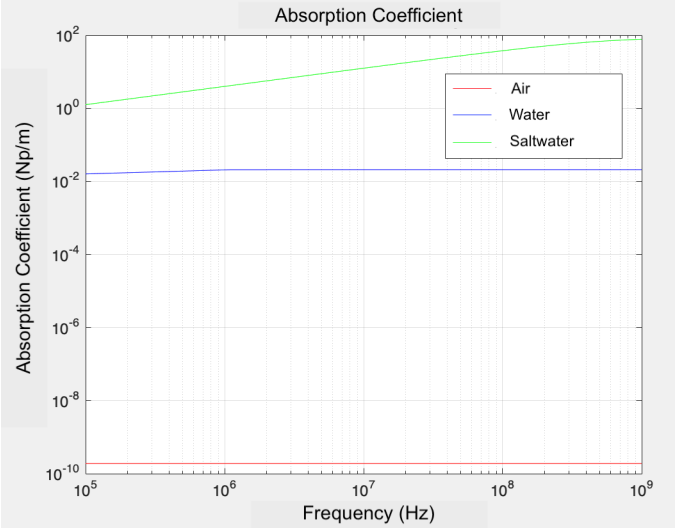

Figure 1. Absorption coefficients of an electromagnetic wave as a function of frequency in different channels.

can be stated that water becomes an excellent dielectric for frequencies above tens of THz.

In Figure 2, the absorption coefficient of electromagnetic waves in a saltwater environment is observed as a function of wavelength. It is noticeable that the lower absorption region is the visible light, more specifically closer to the blue spectrum.

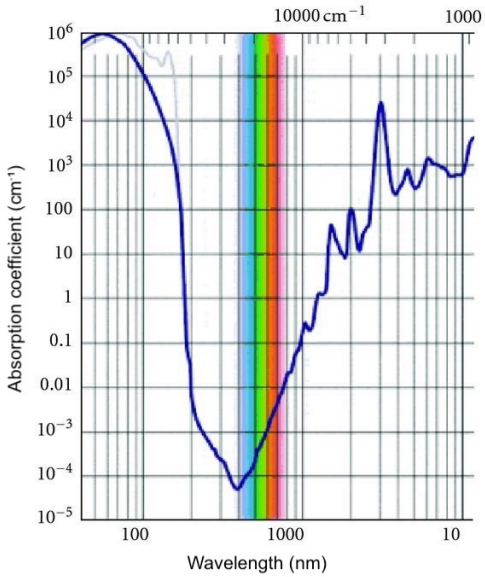

Figure 2. Absorption coefficient of electromagnetic waves in an underwater environment as a function of wavelength. Source: Adapted from Subhash (2012).

However, in different types of bodies of water, the scattering phenomenon promoted by the presence of suspended inorganic particulate and organic matter becomes more relevant than the absorption, which considerably alters the range of wavelengths with the lowest attenuation coefficient, as depicted by Figure 3 below.

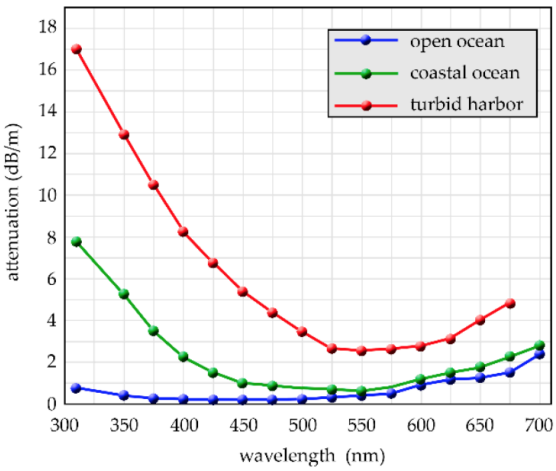

Figure 3. Attenuation coefficient of visible light in different types of bodies of water as a function of wavelength. Source: Schirripa Spagnolo et al. (2020).

3. STATE OF THE ART

In recent years, there has been an increased interest from research institutions and private companies in the development of optical modems for underwater applications. This is mainly due to the advancements in underwater robotics and optoelectronics, especially in the field of emitting devices such as LEDs and lasers, and detecting devices such as photodiodes and photomultipliers (Khalighi et al., 2014). The following section presents the world's most relevant underwater optical modems developed.

3.1 AquaOptical II

The bidirectional optical modem AquaOptical II was developed at the Laboratory of Computer Science and Artificial Intelligence of the Massachusetts Institute of Technology (MIT).

Its photodetector component is an Avalanche Photodiode (APD) connected to an amplifier. The analog signal is converted with a 12-bit Analog to Digital Converter (ADC), which is then sent to a Field Programmable Gate Array (FPGA) and a Central Processing Unit (CPU) for processing.

Its transmitter consists of 18 high-power LEDs, with a spectral band in the range of 470 nm, and their respective driver, producing a luminous power of approximately 10 W. Data is transmitted via Ethernet interface, using User Datagram Protocol (UDP), to the CPU, which then forwards it to the FPGA, responsible for controlling the LEDs driver.

The modems demonstrated good results in tests conducted in a swimming pool, with ambient lighting present, at distances ranging from 7.5 m to 50 m between receiver and transmitter, achieving rates of up to 2.28 Mbps (Doniec and Rus, 2010).

This optical communication system was further refined and patented by the same authors of the aforementioned article (Doniec and Rus, 2015).

3.2 IFREMER optical modem

The renowned French oceanographic research institute, Institut Français de Recherche Pour l'Exploitation de la Mer (IFREMER), developed a unidirectional optical modem in collaboration with the French technology company Osean. This modem was the world's first to be developed using a Silicon Photomultiplier (SiPM) as the photodetector component.

The receiver modem consists of 8 SiPMs, each with a Field Of View (FOV) greater than 30 degrees. The electrical signal from the photomultiplier passes through a high-gain amplifier, a high-speed comparator, and is then sent to an FPGA for demodulation. After this stage, it passes to a board with an ARM architecture processor, and subsequently, the data is made available to the user through an Ethernet interface.

The transmitter modem consists of 120 LEDs arranged in a circular format, generating a luminous beam with a 120-degree aperture. The signal sent by the user through the Ethernet interface, similar to the receiver, passes through the ARM processor, FPGA, and finally to the LEDs driver.

The equipment was field-tested with the support of an ROV. In clear water, without the presence of ambient or artificial lighting, a maximum transmission distance of 60 m was achieved at rates of 3.0 Mbps (Leon et al., 2017).

3.3 BlueComm

Sonardyne is a leading english company in the field of underwater acoustics. In partnership with the Woods Hole Oceanographic Institution (WHOI), it developed a family of optical modems for civilian and military underwater applications (Hub, 2012).

Sonardyne has three main models: the BlueComm 100, the BlueComm 200, and the BlueComm 200 UV. The BlueComm 100 is a bidirectional modem that reaches transmission distances of up to 15 m at speeds of 5 Mbps (Sonardyne, 2016a).

The BlueComm 200 is a unidirectional modem. Its receiver uses a sensitive Photomultiplier Tube (PMT) and has a maximum power consumption of 10 W, with a FOV of 180 degrees. Its transmitter also uses LEDs of 450 nm (royal blue) or 400 - 800 nm (white), with a maximum optical power of 6 W. The maximum transmission distance reported is 150 m in clear waters with very low turbidity and its maximum transmission rate is 10 Mbps (Sonardyne, 2016b).

The BlueComm 200 UV is very similar to the BlueComm 200, but instead it uses LEDs with a wavelength of 405 nm and a receiver with higher responsiveness to the UV spectrum range. This allows the modem to have greater immunity to ambient and artificial light, which facilitates its use near the surface and alongside ROVs. However, it has a shorter transmission range, around 75 m (Sonardyne, 2016c).

IFREMER conducted comparative field tests between its communication system and the BlueComm 200 modem. The tests results are presented in Table 1 below, where different methods of classifying bodies of water, identified

by the Jerlov unit and the Nephelometric Turbidity Unit (NTU), indicate the degree of turbidity present in the environment.

Table 1. Comparative field test results between the IFREMER optical modem and the Sonardyne modem. Source: Leon et al. (2017).

Modem	Water classification (Jerlov)	Water classification (NTU)	Maximum transmission distance (m)
BlueComm 200	5	4	24 (2.5 Mbps)
IFREMER	5	4	17 (3 Mbps)
BlueComm 200	I	0.32	80 (2.5 Mbps)
IFREMER	I	0.32	60 (3 Mbps)

4. DEVELOPMENT

As a development methodology, the transmitter and receiver hardware were designed separately. After simulations and detailed design, a Printed Circuit Board (PCB) model was manufactured, allowing for execution of inumerous bench tests. Further details regarding each of the processes are discussed below.

4.1 Transmitter Hardware

Firstly, an adequate type of phototransmitter for this project was researched. In order to generate a non-collimated beam that could reach the receiving unit without the need for fine adjustment of the line of sight angle between the devices, LEDs of Surface Mount Technology (SMD) technology were used, with a beam aperture of 115 degrees.

In order to reduce the dependence of active thermal management and cooling systems, without significantly reducing the maximum optical power of the transmitter unit, 6 medium-power LEDs were used, each with individual consumption of around 400 mW. The selected LEDs have a known spectral range close to 450 nm, which is minimally attenuated in oceanic and coastal waters, as shown in Figure 3.

For brightness control and digital switching of the LEDs, a specific driver was designed, which implements a voltage-controlled current source, using an operational amplifier. However, to achieve high switching speeds, reaching frequencies of up to tens of MHz, components with higher bandwidth were used. The employed topology is represented by the block diagram in Figure 4.

In order to mitigate the voltage drop across the shunt resistor, which directly affects the current and, consequently, average power dissipation, two groups of phototransmitters were used in parallel, each with three LEDs in series. This also adds robustness to the system by introducing redundancy to the transmitter circuit, maintaining equipment functionality even if one of the LEDs fails in open mode. The overall operation of the circuit was initially verified in the LTSpice XVII simulation environment, with a special focus on the analysis of the current switching

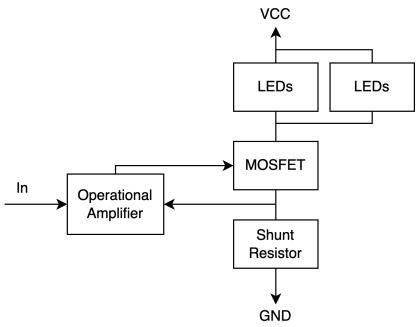

Figure 4. Transmitter circuit simplified block diagram.

behavior in the LEDs, which is directly proportional to the produced optical power.

4.2 Receiver Hardware

A SiPM model manufactured by ON Semiconductor was chosen as the project photoreceiver component due to its low cost and easy of import. The silicon photomultiplier consists of multiple Single Photon Avalanche Detectors (SPADs) along with their quench resistors, arranged in series and parallel, represented by the Figure 5 below.

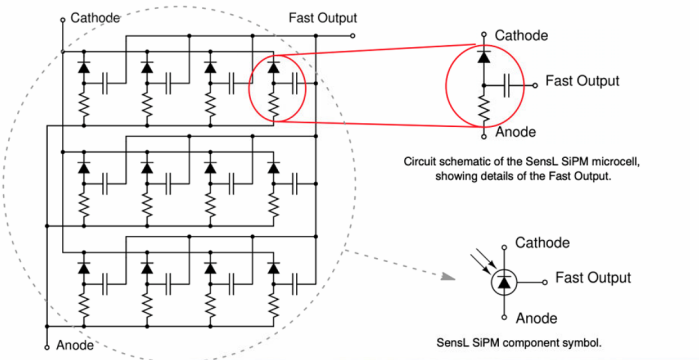

Figure 5. Composition of a SiPM manufactured by the ON Semiconductor company. Source: ONSemi (2021)

In general, it can be stated that each SiPM has on average 100 to 1000 microcells (highlighted in red in Figure 5) per mm^2. Thus, each microcell detects photons independently, and the electrical currents generated by each of the APDs in parallel are summed, producing an analog output capable of providing data related to the instantaneous magnitude of the incident optical power.

SiPMs are compact, robust, immune to external magnetic fields, relatively low cost, and have high gain, controlled by their bias voltage. However, these photomultipliers, which have only recently been widely available on the market, have several sources of intrinsic noise, and their response to light pulses has a complex multi-exponential shape (Ching-Roa et al., 2021). Some types of noise present in SiPMs can be observed in Figure 6 below.

To control the gain and limit the maximum current consumed by the SiPM, a hardware-based Automatic Gain Control (AGC) was designed, which directly affects the bias voltage of the SiPM through the use of an operational amplifier and a Field Effect Transistor (FET). In the Fast output, a non-inverting amplifier was implemented,

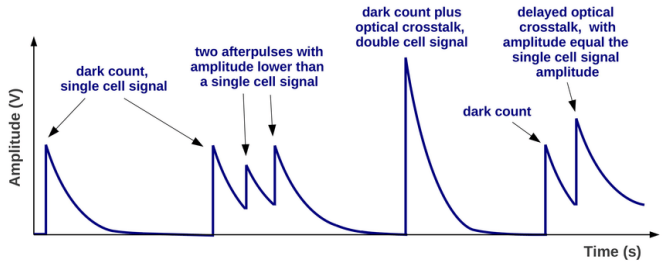

Figure 6. Representation of negative effects related to noise sources. Source: Gundacker and Heering (2020)

followed by a hysteresis comparator, for the digitization of the received signals. This topology, which allows gains on the order of 10^9, is represented by the diagram in Figure 7.

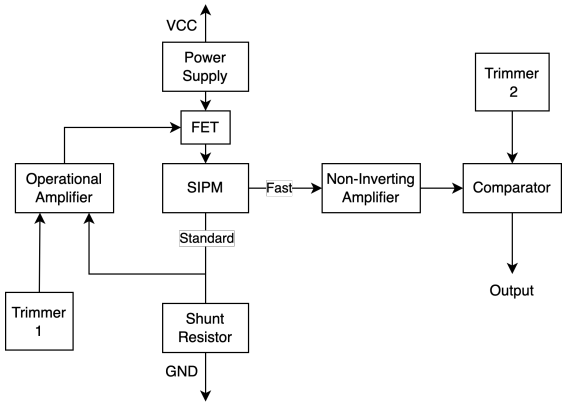

Figure 7. Receiver circuit simplified block diagram.

The behaviour of the AGC, amplification and digitization subcircuits were verified separately through simulations conducted in the LTSpice XVII software.

4.3 PCB

After refining phases of the transmitter and receiver circuits development, PCBs for both electronics were designed using Altium 21 software, which allowed for cost reduction in manufacturing and production of hardware capable bidirectional devices. The finalized PCB design is represented by Figure 8.

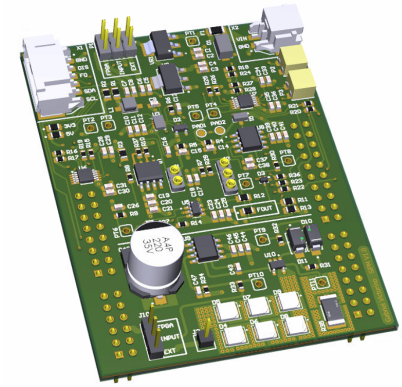

Figure 8. PCB 3D image.

4.4 Bench tests

Initially, the transmitter circuit was verified using an arbitrary signal generator and an oscilloscope. The circuit was validated for frequencies up to 10 MHz by injecting an input signal, represented by a square wave, and measuring the current through the shunt resistor, which exhibited a wave behaviour similar to the ones obtained in LTSpice XVII.

In the receiver circuit, the AGC was first validated to ensure the operation and protection of the SiPM. After this step, the operation of the amplification and digitization circuit was verified, as shown in Figure 9. When analyzing the behavior of the Fast output in the presence of reduced ambient light, various spikes were observed at the amplification stage (green) and at the digitized output (yellow), even without current flowing through the LEDs (purple).

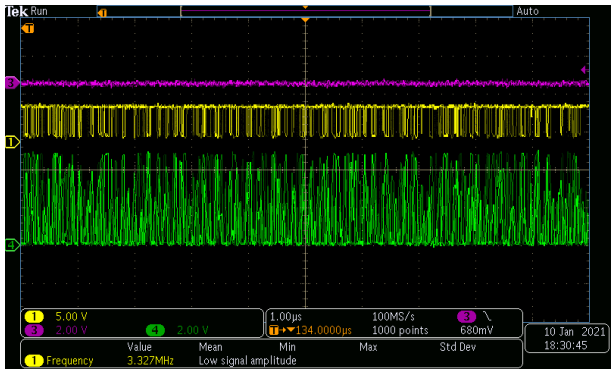

Figure 9. SIPM response test in the presence of low incident light, displaying the current consumed by the LEDs (purple), the sensor output after amplification (green), and the SiPM digitized output (yellow).

These spikes are generated by the increase in gain imposed by the AGC due to the low incident illumination. The increased gain considerably raises the Dark Count Rate (DCR), optical crosstalk, and afterpulsing, resulting in unexpected spikes, as depicted in Figure 6. Additionally, as the tests were not conducted in a dark chamber, some of the spikes may have originated from genuine photon detections. The amplified spikes, with amplitudes close to 5 V, were detected by the comparator circuit, which relayed them to the digital output. On the other hand, with the increase of ambient illumination, a considerable reduction in the spike amplitude was observed, justified by the decrease in gain imposed by the AGC.

Afterwards, integrated tests were conducted with the usage of the transmitter PCB, which demonstrated that the LEDs brightness saturate the SIPM momentarily, ceasing the production of spikes for a certain amount of time, as shown in Figure 10. This behaviour demonstrates that the induced spikes could be avoided if the encoded message continuously produced light pulses, regardless of the data content.

It was also observed that the pulse width of the receiver output is practically constant, regardless of the luminous pulse width produced by the LED.s This behavior is explained by the presence of series capacitors in the Fast

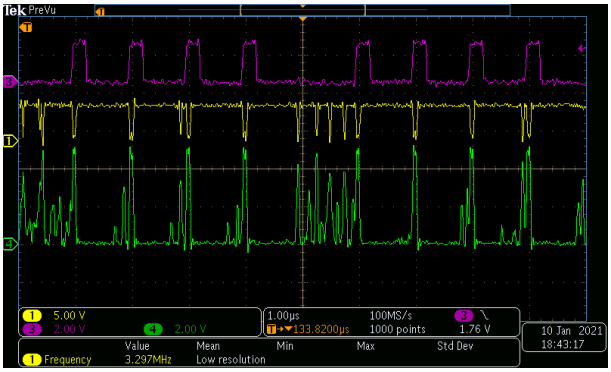

Figure 10. SIPM response test in the presence of transmitter incident light pulses, displaying the current consumed by the LEDs (purple), the sensor output after amplification (green), and the SiPM digitized output (yellow).

output of this SiPM model. These operating characteristics and the difficulty in processing the SiPM electrical signals are also briefly discussed in Leon et al. (2017), where the authors mention that the solution found to mitigate the negative effects presented were the usage of a modulation with very fast light pulses and the implementation of a hardware AGC.

4.5 Modulation

To mitigate the discussed SIPM negative effects, different types of digital modulation found in the literature were analyzed, but only the Discrete Pulse Interval Modulation (DPIM) could natively handle the detection of pulses with fixed width and the generation of pulses during the translation of bit 0. However, due to the nature of this modulation technique, which varies the enconding packet size based not only on the data length, but also on the data content, the DPIM was not selected to this project. Instead, an adaptation of the Manchester encoding was employed in the receiver unit. An example of the developed modulation is represented by Figure 11, where bit 0 is represented by the transition $0 \rightarrow 0 \rightarrow 1$ and bit 1 is represented by the transition $0 \rightarrow 1 \rightarrow 0$.

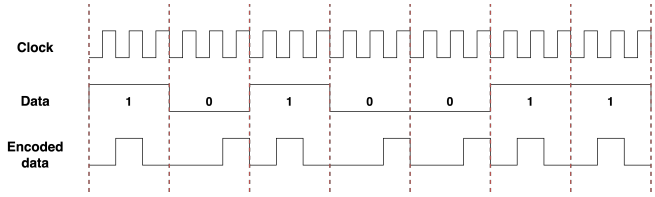

Figure 11. Developed encoding applied to an arbitrary data stream.

As Figure 11 shows, the developed encoding always generates pulses of fixed width, regardless of the data content. However, this modulation technique has lower efficiency compared to Manchester encoding, as it requires three clock pulses to transmit 1 bit of data. Furthermore, it does not have a transfer function based on simple logical operations, which adds complexity to the development.

A transmission protocol was also defined, including a start bit and a parity bit, to increase the communication integrity.

4.6 Integration

Given the magnitude of the transmission frequencies and the costly process of modulation and demodulation, the use of an FPGA for the design of modulation and demodulation blocks, written in VHSIC Hardware Description Language (VHDL), is justified. For this purpose, Arty Z7 development kits were used.

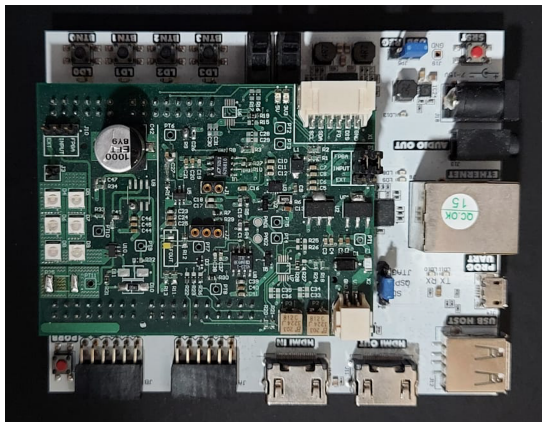

Figure 12. Arty Z7 kit integrated to the dedicated hardware developed.

The Zynq-7000 chip in the Arty Z7 is a System on Chip (SoC), which consists of an ARM Cortex-A9 processor, with a maximum clock frequency of 650 MHz, and a Xilinx Series 7 FPGA. The integration between the developed PCB and the ARTY Z7 is achieved through the connection of the male and female headers present on each one of the boards, as shown in Figure 12.

The system operation is initiated by sending messages to the transmitter device through the Ethernet interface. The ARM processor, present in the SoC, interprets the data through the Lightweight IP (LwIP) stack, implemented in the C language. The TCP/IP stack then transmits the messages to a First In First Out (FIFO) buffer, which directs them continuously to the modulator implemented in VHDL on the FPGA. The modulator, in turn, assembles the modulated packets and it generates a digital signal that controls the LED driver.

Upon receiving the light stimulus, the receiver device sends the analog signal to the amplification and digitization electronics. After this process, the digital signal is directed to the demodulator, which implements the decoding. The decoded signal is then sent to a FIFO buffer, responsible for triggering the LwIP library, which facilitates the transmission of data to the user through the Ethernet interface. The simplified block diagram of the developed optical communication system is shown in Figure 13.

5. EXPERIMENTAL RESULTS

Firstly, it was necessary to assemble the electronic boards in a waterproof housing, in order to conduct communication tests with the submerged transmitter and receiver modems. For this purpose, two watertight cylindrical aluminum vessels with acrylic windows were designed and manufactured. Moreover, to transmit data and power to

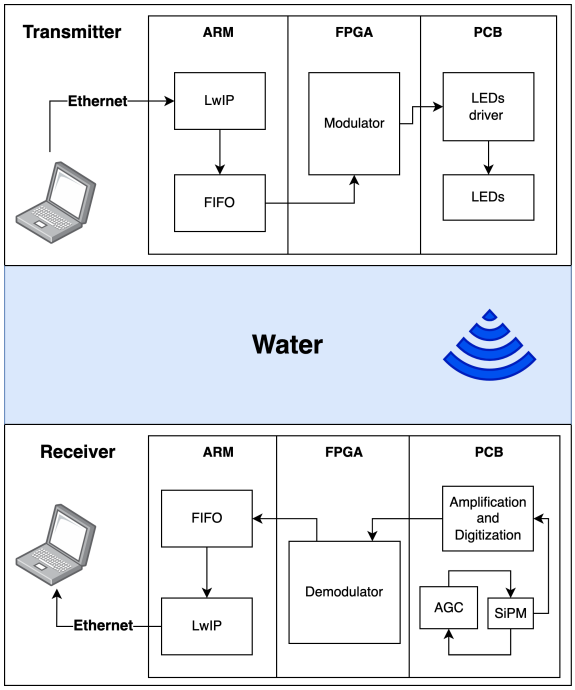

Figure 13. Communication system simplified block diagram.

the embedded electronics, special subsea bulkhead connectors were employed, as shown in Figure 14.

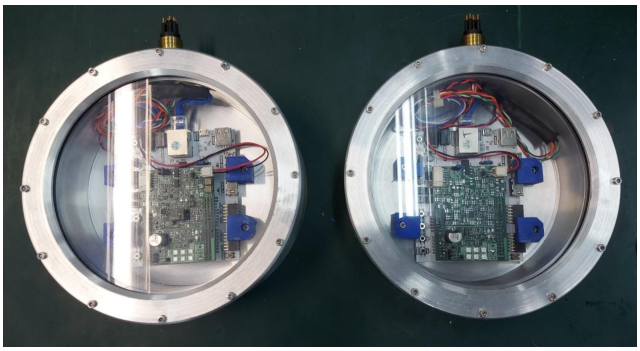

Figure 14. Optical transmitter and receiver devices assembled inside the waterproof vessels.

For the communication tests preparation in a submerged environment with reduced external light intensity, a hyperbaric chamber was used. The vessels were positioned with a direct line of sight above a wooden structure, allowing for tests with different distances between modems to be conducted. The described setup can be seen in Figure 15.

For the communication test execution, two Python v3.10 applications were written. One for the transmitter, responsible for sending a 30 Mbit packet at a rate of 2.4 Mbps, and another for the receiver, tasked with verifying the integrity of the message and counting the collected bytes. Thus, it was possible to obtain a Bit Error Rate (BER) for each transmission distance.

Three BER experiments were conducted for each one of the three defined distances between transmitter and receiver modems (2.5 m, 1.5 m, and 0.5 m). The mean and standard deviation of the BER for each case is stated in Table 2.

Figure 15. Underwater experiment assemble.

Table 2. Mean and standard deviation of the BER for different distances between transmitter and receiver modems.

Distance between modems (m)	**BER mean (%)**	**BER standard deviation (%)**
2.5	39.18	0.27
1.5	15.47	0.13
0.5	0.00	0.00

Firstly, a drastic increase in the BER was observed with the transmission distance increase. This result was expected and can be explained by several factors, such as the reduction of optical power detected by the photoreceptor due to attenuation caused by water and suspended particles, reflection of light on the inner walls of the hyperbaric chamber, which have white color and glossy finish and can cause intersymbolic interference during the demodulation process, as well as the increase in gain applied by the AGC, which increases the intrinsic noise of the SiPM, producing spikes that interfere with the detection of optical signals from the transmitter. However, for short distances like 0.5 m, there was no packet loss during the experiment, demonstrating the full operation of the constructed prototypes.

6. CONCLUSION

The studies conducted on the topic of optical communication, along with the research of equipments developed by universities, institutes, and private companies, assisted in defining the boundary conditions and achievable objectives for the development of an unidirectional underwater optical communication system capable of data transfers at rates above 1 Mbps, at distances of a few meters.

For the development of the receiver system, the use of a relatively new type of photoreceptor called SiPM was highlighted, which is capable of providing information regarding the absorbed optical power and the photon arrival time. Although widely used in photon counting applications, the use of this sensor in underwater optical receivers was only found in an international article regarding the IFREMER optical modem.

A specific analog output of the SiPM was explored, which supposedly allows an increase in the transmission bandwidth. However, it was found during experiments that several intrinsic characteristics related to noise caused by

optical and thermodynamic effects make its use difficult for the application, especially in a heterogeneous, uncharacterized medium such as water. To mitigate these negative and secondary effects of the sensor, a specific modulation technique was designed based on the tests conducted.

After complete implementation of the system, which included the development of waterproofing vessels, data transfer with three transmission distances in a hyperbaric chamber full of water were carried out to analyze the overall BER. The prototypes produced enabled the establishment of unidirectional data transmission at speeds of 2.4 Mbps at distances of up to 2.5 meters.

Among the future works, the analysis of the BER under different variables such as light interference and water turbidity are highlighted. Additionally, the study and design of different modulation techniques, the use of sophisticated error correction protocols and the development of bidirectional devices are mentioned.

ACKNOWLEDGEMENTS

The authors would like to thank the Unmanned Vehicles Laboratory of the University of São Paulo for the technical support and for the infrastructure provided for conducting the experiments. This study was financed in part by the Coordenação de Aperfeiçoamento de Pessoal de Nível Superior – Brasil (CAPES) – Finance Code 001.

REFERENCES

Balanis, C.A. (2012). *Advanced engineering electromagnetics*. John Wiley & Sons.

Ching-Roa, V.D., Olson, E.M., Ibrahim, S.F., Torres, R., and Giacomelli, M.G. (2021). Ultrahigh-speed point scanning two-photon microscopy using high dynamic range silicon photomultipliers. *Scientific Reports*, 11(1), 1–12.

Doniec, M. and Rus, D. (2010). Bidirectional optical communication with aquaoptical ii. In *2010 IEEE International Conference on Communication Systems*, 390–394. IEEE.

Doniec, M.W. and Rus, D. (2015). Underwater optical communication system. US Patent 9,031,413.

Gundacker, S. and Heering, A. (2020). The silicon photomultiplier: fundamentals and applications of a modern solid-state photon detector. *Physics in Medicine & Biology*, 65(17), 17TR01.

Gussen, C.M., Diniz, P.S., Campos, M.L., Martins, W.A., Costa, F.M., and Gois, J.N. (2016). A survey of underwater wireless communication technologies. *J. Commun. Inf. Sys.*, 31(1), 242–255.

Hub, G.U. (2012). Sonardyne Announces Collaboration With WHOI Engineers. Disponível em: `https://www.globalunderwaterhub.com/2980/sonardyne-announces-collaboration-with-whoi-engineers-to-launch-subsea-optical-communication-technology`.

Khalighi, M.A., Gabriel, C., Hamza, T., Bourennane, S., Leon, P., and Rigaud, V. (2014). Underwater wireless optical communication; recent advances and remaining challenges. In *2014 16th International Conference on Transparent Optical Networks (ICTON)*, 1–4. IEEE.

Lehman, J. (2018). From ships to robots: The social relations of sensing the world ocean. *Social studies of science*, 48(1), 57–79.

Leon, P., Roland, F., Brignone, L., Opderbecke, J., Greer, J., Khalighi, M., Hamza, T., Bourennane, S., and Bigand, M. (2017). A new underwater optical modem based on highly sensitive silicon photomultipliers. In *OCEANS 2017-Aberdeen*, 1–6. IEEE.

List, C.C. (2017). USA Control List. Disponível em: `https://www.bis.doc.gov/index.php/documents/regulations-docs/federal-register-notices/federal-register-2014/950-ccl5-pt1/file`.

Mariano, J. and La Rovere, E. (2007). Oil and gas exploration and production activities in brazil: The consideration of environmental issues in the bidding rounds promoted by the national petroleum agency. *Energy Policy*, 35(5), 2899–2911.

ONSemi (2021). Introduction to the Silicon Photomultiplier (SiPM). Disponível em: `https://www.onsemi.com/pub/Collateral/AND9770-D.PDF`. Acesso em: 29/01/2022.

Schirripa Spagnolo, G., Cozzella, L., and Leccese, F. (2020). Underwater optical wireless communications: Overview. *Sensors*, 20(8), 2261.

Somaraju, R. and Trumpf, J. (2006). Frequency, temperature and salinity variation of the permittivity of seawater. *IEEE transactions on Antennas and Propagation*, 54(11), 3441–3448.

Sonardyne (2016a). Bluecomm 100 Datasheet. Disponível em: `https://www.sonardyne.com/app/uploads/2016/06/Sonardyne_8360_BlueComm_100.pdf`.

Sonardyne (2016b). Bluecomm 200 Datasheet. Disponível em: `https://www.sonardyne.com/app/uploads/2016/06/Sonardyne_8361_BlueComm_200-1.pdf`.

Sonardyne (2016c). Bluecomm 200 UV Datasheet. Disponível em: `https://www.sonardyne.com/app/uploads/2016/06/Sonardyne_8361_BlueComm_200_UV.pdf`.

Subhash, H.M. (2012). Full-field and single-shot full-field optical coherence tomography: a novel technique for biomedical imaging applications. *Advances in Optical Technologies*, 2012.

Tyler, R.H., Sanford, T.B., and Unsworth, M.J. (1998). Propagation of electromagnetic fields in the coastal ocean with applications to underwater navigation and communication. *Radio Science*, 33(4), 967–987.

Union, O.J.E. (2016). EU Control List. Disponível em: `https://danishbusinessauthority.dk/sites/default/files/media/annex_i_reg._2016-1969.pdf`.

Yuh, J., Marani, G., and Blidberg, D.R. (2011). Applications of marine robotic vehicles. *Intelligent service robotics*, 4(4), 221–231.

Zhang, F., Marani, G., Smith, R.N., and Choi, H.T. (2015). Future trends in marine robotics [tc spotlight]. *IEEE Robotics & Automation Magazine*, 22(1), 14–122.